ARTICLE

A Stable, Label-free Optical Interferometric Biosensor Based on TiO_2 Nanotube Arrays

Kyu-Shik Mun,[†] Sara D. Alvarez,[‡] Won-Youl Choi,[†,*] and Michael J. Sailor[‡,*]

[†]Department of Metal and Materials Engineering Kangnung National University 120 Kangnung Daehangno, Kangnung 210-702, Korea, and [‡]Department of Chemistry and Biochemistry University of California, San Diego 9500 Gilman, La Jolla, California 92093

ABSTRACT Optical interferometry of a thin film array of titanium dioxide (TiO_2) nanotubes allows the label-free sensing of rabbit immunoglobulin G (IgG). A protein A capture probe is used, which is immobilized on the inner pore walls of the nanotubes by electrostatic adsorption. Control experiments using IgG from chicken (which does not bind to protein A) confirms the specificity of the protein A-modified TiO_2 nanotube array sensor. The aqueous stability of the TiO_2 nanotube array was examined and compared with porous silica (SiO_2), a more extensively studied thin film optical biosensor. The TiO_2 nanotube array is stable in the pH range 2 to 12, whereas the porous SiO_2 sensor displays significant degradation at pH > 8.

KEYWORDS: TiO_2 · porous silicon · nanotubes · optical biosensor · immunosensor · interferometry

Label-free biosensors allow monitoring of biomolecular interactions in real-time without a molecular marker and are desired for applications in disease diagnostics, drug discovery, environmental monitoring, and food safety.[1−6] Various label-free biosensors have been developed to provide simple and rapid detection by converting biomolecular interactions into optical, electrical, thermal, or acoustic signals.[7−10] For label-free optical biosensors,[11,12] the transduction methods can be divided into two categories: optical interferometric[13−15] and surface plasmon methods.[16−18]

Porous silicon has been demonstrated to be an effective optical interferometric sensing material because of its large internal surface area, ease of fabrication, and its chemically modifiable surface.[2,19−22] However, a significant limitation of the porous silicon system is stability.[2] Freshly etched porous Si contains surface Si−H groups that readily oxidize in aqueous media resulting in degradation of the surface. Chemical modification with Si−O or Si−C linkages provides substantial improvement in stability under low pH conditions; however, within the physiological and higher pH range porous silicon surfaces are subject to various degrees of corrosion and dissolution, which can produce unacceptable zero-point drift when used as a biosensor.[2,23,24] In an attempt to find porous materials that might be more stable in aqueous media, we recently reported an optical biosensor made of porous alumina (Al_2O_3).[25] This device used antibody capture probes and was found to be more stable than porous Si or SiO_2-based systems, while retaining the high sensitivity of the optical interferometric method. While stable at pH 7, porous alumina is amphoteric, with a limited pH range over which it is stable. The discovery of porous forms of titanium oxide (TiO_2), in particular TiO_2 nanotube arrays, provides another candidate material for an optical sensor.[6,26−29] In addition to its greater aqueous stability, TiO_2 possesses a larger index of refraction than either Al_2O_3 or SiO_2 (n = 2.5 *vs* 1.65 or 1.7, respectively[30−32]). The larger index contrast between the porous host and the aqueous matrix in which the biomolecular binding measurement is carried out is expected to provide greater contrast in the interferometric spectrum, leading to lower noise and higher sensitivity.

Prepared from titanium (Ti) metal using anodic oxidation,[27,33−36] TiO_2 nanotube arrays have attracted significant interest for solar cell, drug delivery, and lithium-ion battery applications owing to their large surface area and well-ordered, stable structures.[27,33,37−41] Most recently, an antibody-based sensor using optical reflectivity from a TiO_2 nanotube array was demonstrated.[26] We hypothesized that the large internal surface area, the negative surface charge,[6,42] and the high effective refractive index of TiO_2 nanotube arrays could allow

*Address correspondence to cwy@kangnung.ac.kr, msailor@ucsd.edu.

Received for review September 28, 2009 and accepted March 24, 2010.

Published online March 31, 2010. 10.1021/nn901312f

TABLE 1. Properties of Porous SiO_2 and TiO_2 Samples Used in This Study[a]

sample	thickness (μm)	porosity (%)	pore diameter (nm)	optical thickness, *nL* (nm)	
				air	ethanol
TiO_2	6.71 ± 0.15	40 ± 1	100	12 600 ± 200	13 600 ± 300
SiO_2	6.69 ± 0.03	49 ± 1	30	9 000 ± 200	10 300 ± 300

[a]Thickness and porosity values determined from SLIM analysis as described in the text. Nominal average pore diameters determined by SEM. Results are means ± standard deviation of the mean of three porous samples. One measurement was obtained from each sample.

convenient incorporation of biomolecules and high analyte sensitivity. In this work, we demonstrate the use of TiO_2 nanotube arrays for label-free optical interferometric biosensing using a protein A capture probe and an immunoglobulin G (IgG) analyte. We investigate the fundamental response of the material to liquid infiltration and compare the aqueous stability of porous TiO_2 to porous silica (SiO_2) in the pH range 2−12.

TiO_2 nanotube arrays and porous SiO_2 with similar values of thickness and porosity (within 10%) were prepared (Table 1). Porous SiO_2 was prepared by thermal oxidation of electrochemically etched porous Si samples.[43] The setup for the biosensing and aqueous stability experiments is shown in Figure 1 and consists of a thin film of porous TiO_2 or porous SiO_2 mounted in a transparent poly(methyl)methacrylate flow cell. Reflectance spectra were collected and transmitted through fiber optic cables as previously described.[43]

The reflectance spectrum consists of fringes due to thin-film Fabry−Perot interference. Sensing is achieved by extracting the refractive index of the porous matrix by applying a fast Fourier transform (FFT) to the fre-

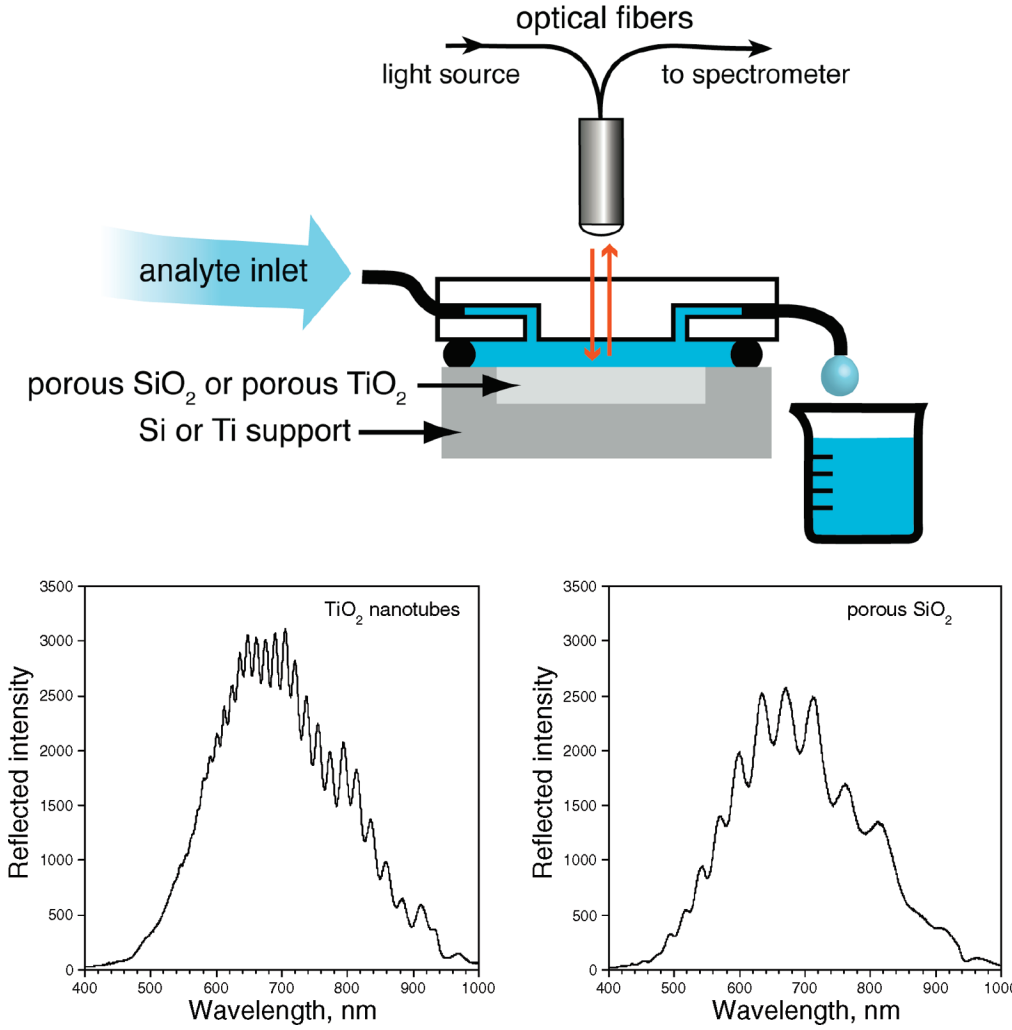

Figure 1. Schematic diagram of the flow cell setup used in stability and biosensing experiments, and representative reflectivity spectra of porous SiO_2 and TiO_2 nanotube samples showing the characteristic interference fringes. Each sample is illuminated with focused white light, and reflected light is collected through the same lens positioned along an axis normal to the sensor surface, and transmitted to a CCD spectrometer. The reflectivity spectra shown were obtained with the samples immersed in phosphate buffered saline solution at pH 7.4, and they are uncorrected for instrumental spectral response.

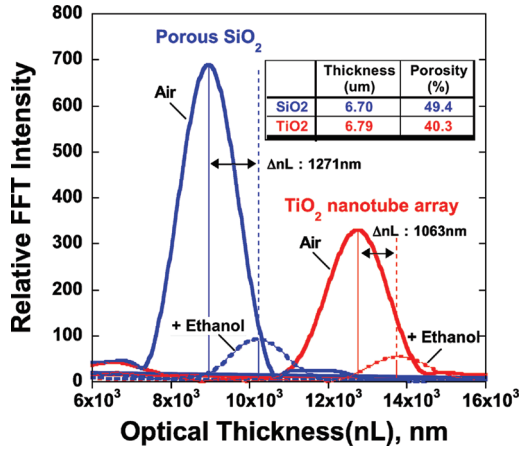

Figure 2. Reflective interferometric Fourier transform spectroscopy (RIFTS) data obtained by Fourier transform of the reflectivity spectra from a porous SiO_2 thin film (blue) and TiO_2 nanotube array (red). Spectra were obtained from samples in air (solid traces) and immersed in ethanol (dashed traces). Red shifts in the reflectivity spectra correspond to changes in refractive index of the porous films upon replacement of air ($n = 1$) with ethanol ($n = 1.3611$).

quency reflectance spectrum. The method is referred to as reflective interferometric Fourier transform spectroscopy (RIFTS).[44] Details of the Fourier transform and spectral data fitting routines are published elsewhere.[45] Figure 2 presents the RIFTS spectra obtained from representative porous SiO_2 and porous TiO_2 films in air and the corresponding spectra of the films submerged in neat ethanol.

The position of the peak along the *x*-axis in the RIFTS spectrum corresponds to the optical thickness, *nL*, where *n* and *L* are the total refractive index and thickness of the porous layer, respectively. The total refractive index is a composite refractive index of the as-prepared TiO_2 or SiO_2 component and any material residing within the pores; in this case, air or ethanol. The porosity and thickness of the films can be determined using the spectroscopic liquid infiltration method (SLIM):[46] The change in optical thickness determined from the film filled with air and with ethanol is least-squares fit to a two-component Bruggeman effective medium approximation. The values of porosity and thickness calculated using the SLIM approximation for representative porous SiO_2 and TiO_2 samples are presented in Figure 2 (inset), and averages of three samples are presented in Table 1.

The value of *nL* is significantly larger for the TiO_2 film relative to the SiO_2 film, and this is a consequence of the larger index of refraction of TiO_2 ($n = 2.5$) *versus* SiO_2 ($n = 1.7$)[30,32] and the lower porosity of the TiO_2 sample. The addition of ethanol ($n = 1.3611$) causes an increase in position and a decrease in amplitude of the RIFTS spectral peak for both TiO_2 and SiO_2 films. The percent change in optical thickness of the porous TiO_2 film ($\Delta OT/OT_{air}$, 7.75%) is less than that of porous SiO_2 (12.40%). The larger percent change in OT of the porous SiO_2 samples is due to the larger porosity of the SiO_2 samples (49%) *versus* the TiO_2 nanotube arrays (39%). In both samples there is a significant decrease in intensity of the RIFTS peak upon immersion in ethanol, representative of the decrease in index contrast between the porous host matrix and the filling medium. This intensity decrease is less severe for the porous TiO_2 system because of the larger refractive index of TiO_2 relative to SiO_2.

The stability of the TiO_2 nanotube arrays was quantified in various buffer solutions covering the pH range 2−12. The buffers were introduced at a flow rate of ~0.7 mL/min and the spectral responses recorded. The value of *nL* (optical thickness) obtained from the RIFTS spectrum as described above are presented in Figure 3. The refractive index of each buffer was measured independently with a refractometer and they were all close to the value of 1.3345 recorded for the pH 7.4 buffer at 22 °C (phosphate buffered saline solution, PBS). At pH values <5, the optical thickness of the porous SiO_2 layer tracks well with the refractive index of the corresponding buffer solutions. However, for buffer solutions with pH > 8, a significant time-dependent decrease from the baseline *nL* value is observed, and the measured *nL* value no longer tracks the refractive index of each buffer solution. This result is caused by degradation of the SiO_2 matrix in basic solutions and demonstrates the poor utility of porous SiO_2 sensors at pH > 8. In contrast, the optical thickness value measured from the TiO_2 nanotube arrays consistently follows the refractive index of each buffer solution, and the baseline is stable over the entire pH range studied.

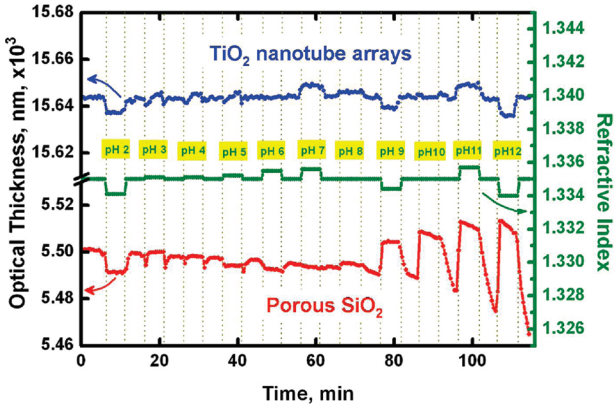

Figure 3. Optical thickness response curves of TiO_2 nanotube arrays and porous SiO_2 upon exposure to buffer solutions in the range pH = 2−12. The cell was flushed with pH 7.4 PBS buffer solution between each buffer exposure.

The morphology of the TiO_2 nanotube array was examined by scanning electron microscopy (SEM, Figure 4) before and after the pH stability tests represented by Figure 3 were performed. The porous TiO_2 layer shows a highly ordered nanotube array structure, with an aspect ratio of ~70. The thickness (~7 μm) and pore size (~100 nm) of the nanotube arrays is maintained after exposure to the test solutions of the pH stability experiments. The lack of microstructural degradation of the

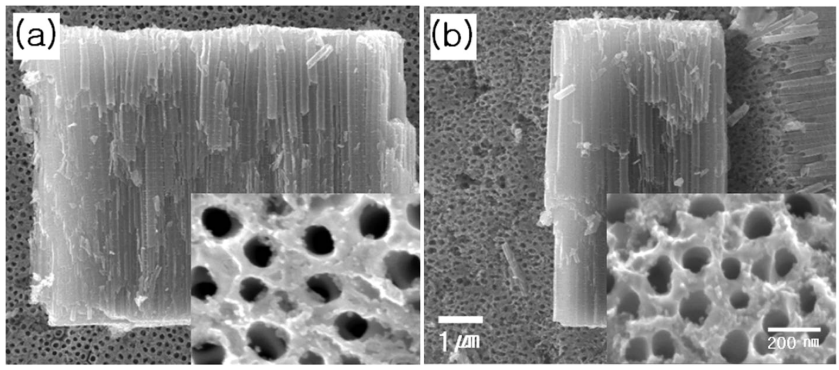

Figure 4. Field emission scanning electron microscope (FESEM) images of TiO_2 nanotube arrays before (a) and after (b) the pH stability experiments of Figure 3. Film fragments are shown in cross-section in the main images; close-up, plan-view images are shown in the insets.

TiO_2 nanotube arrays supports the optical interferometric measurements, indicating that the material is stable in the pH range 2−12.

Specific biomolecular binding experiments were performed using a protein A (MW ≈ 42 kDa) capture probe and immunoglobulin G (IgG, MW ≈ 150 kDa) analyte. Protein A is derived from *Staphylococcus aureus* bacteria and is part of a small collection of proteins known to specifically bind to the Fc domain of a number of antibodies. The antibody binding affinity of protein A is species specific; it has a strong affinity for IgG derived from rabbits, but it will not bind chicken IgG.[47] The interactions were observed by time-resolved measurement of optical thickness as the different proteins were introduced into the flow cell (Figure 5). To establish a baseline, PBS buffer solution was introduced to the cell containing the nanotube array sample and allowed to equilibrate for several minutes. A solution of 0.1 mg/mL protein A in PBS buffer was then introduced, and the solution was allowed to circulate under continuous flow for 1 h. An increase in the measured value of optical thickness of 50 nm was observed during this period, indicating that protein A is electrostatically adsorbed to the negatively charged surface[6,42] of the TiO_2 nanotubes.[48,49] Rinsing with PBS buffer produces a small decrease in optical thickness of ~3 nm, due to removal of unbound or weakly bound protein A-IgG complex from the TiO_2 nanotube arrays.

The protein A that was electrostatically bound to the TiO_2 nanotube array was removed with a surfactant solution and quantified using a colorimetric protein assay (bicinchoninic acid, BCA). Typical loading values were 46 μg in a sample, corresponding to a mass loading of 15% (180 μg of protein per mg of TiO_2), or a volumetric loading of 115 mg/mL (mg of protein A contained per mL of apparent volume). The optical measurement yields a somewhat lower value of 46.1 mg/mL for the volumetric loading of protein. The optical measurement assumes a density of 1.17 g/mL and a refractive index of 1.47 for protein A.[50] Relative to the traces of Figures 5 and 6, the amount of protein present in the sample is thus 1−2 μg per nm of shift in the value of optical thickness (*nL*). The detection limit of the system corresponds to 14 ng of protein in the ~1 mm diameter cylindrical volume probed by the optics.

Introduction of a solution containing 0.1 mg/mL of rabbit IgG results in an increase in optical thickness of ~20 nm. This change in optical thickness is attributed to specific binding between protein A and rabbit IgG based on a control experiment performed with non-binding chicken IgG (see below). However, the rate of increase in optical thickness upon binding is slower in comparison to IgG binding curves obtained in the porous SiO_2 system,[43] indicating slow diffusion of the large antibody (150 kDa) into the protein A-coated pores of the TiO_2 nanotube arrays. A subsequent rinse with PBS buffer showed no change in optical thickness, demonstrating the strong binding affinity between protein A and rabbit IgG.

To confirm that the change in optical thickness was due to specific binding between protein A and rabbit IgG, IgG from chicken was introduced to a protein A-modified TiO_2 nanotube array (Figure 6). It is known that protein A does not bind chicken IgG, and no change in optical thickness is observed in this experiment. However, when chicken IgG is introduced to bare TiO_2 nanotube arrays (not containing a protein A cap-

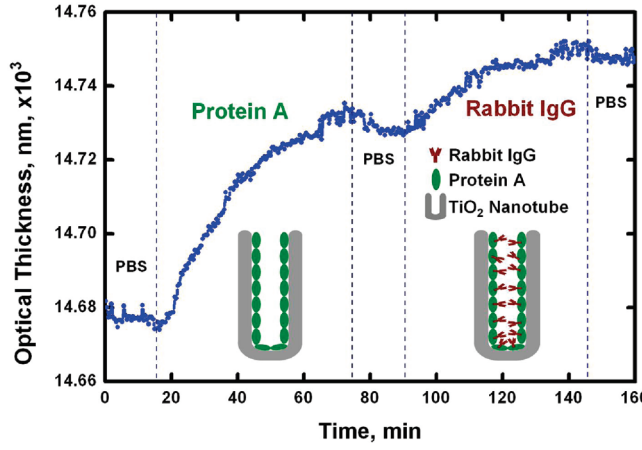

Figure 5. Time-dependent optical thickness measurements showing sequential binding of Protein A and rabbit IgG within TiO_2 nanotubes.

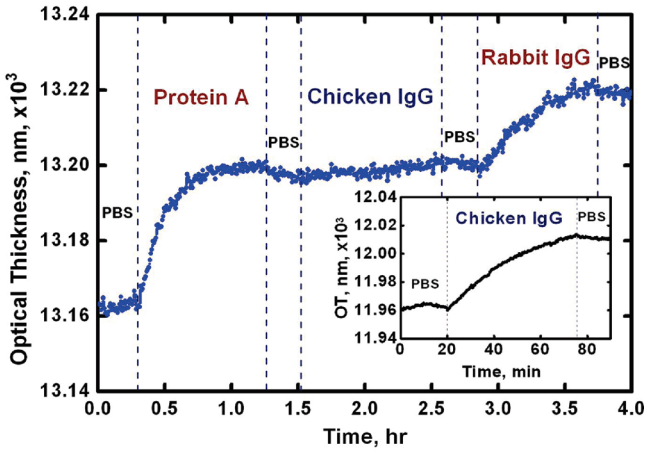

Figure 6. Binding profile for TiO_2 nanotube array sequentially exposed to protein A, chicken IgG, and then rabbit IgG. The inset shows time-dependent binding curve of a bare TiO_2 nanotube array (no protein A adsorbed) exposed to chicken IgG.

ture probe), an increase in optical thickness of ~50 nm is observed. This demonstrates that chicken IgG will strongly adsorb to the negatively charged internal surface of bare TiO_2 nanotube arrays (Figure 6 inset), but not to protein A-modified TiO_2 nanotubes. The combined results show that the surface of TiO_2 nanotube arrays can be sufficiently covered by protein A that the nonspecific binding of other proteins (IgG in this case) is inhibited.

The protein A-coated surface remains selective for rabbit IgG, indicating that the strong interaction of protein A with TiO_2 does not completely inactivate this protein's ability to bind IgG. However, only a relatively small fraction of protein A on the porous TiO_2 surface participates in IgG binding. The interferometric measurement produces an optical thickness signal that scales with analyte mass,[2] and so the data can be used to estimate the mass fraction of active protein A. If all the protein A on the surface were active, the magnitude of the optical thickness change expected for binding of (rabbit) IgG is expected to be ~180 nm (50 nm shift for protein A multiplied by the mass ratio of protein A/IgG = 50 × 150/42). The observed shift for rabbit IgG binding of ~20 nm suggests that only 10% of the protein A bound to the surface is able to bind IgG. This lower binding activity is attributed to a combination of two factors: (1) some of the protein A molecules are oriented with their IgG binding domain face-down, or in a suboptimal orientation on the TiO_2 surface; and (2) binding to the TiO_2 surface results in partial denaturation of protein A, negating its ability to bind IgG.

In summary, the reflectivity spectra of anodized TiO_2 nanotube arrays display optical interference fringes that efficiently report infiltration of liquids and adsorption of molecules from solution. TiO_2 nanotube arrays display superior chemical stability in the pH range 2−12 in comparison to porous SiO_2, which degrades in basic solutions, or porous Al_2O_3, which is unstable in acidic conditions. The stability of TiO_2 nanotube arrays suggests that the material is appropriate for sensor applications involving a wide range of acidic, basic, and physiological pH conditions. The surface affinity of porous TiO_2 is sufficient to allow strong noncovalent binding of the capture probe protein A, which can then act as a specific and effective sensor for IgG. Adsorption of protein A is attributed to electrostatic interactions between the negatively charged TiO_2 surface and the protein, and it effectively minimizes the nonspecific binding of proteins subsequently introduced. While not demonstrated in this work, the ability of the material to capture IgG enables the use of anodized TiO_2 thin films in a cascaded sensing scheme, in which the captured IgG antibody can then become the capture probe for an additional target analyte in an immunoassay.[25] For the protein A/IgG system, analyte diffusion into the pores is slower than the fundamental binding rate of protein A to IgG, which places a lower limit on the response time of the sensor and on the ability of this system to yield kinetic binding constants.

EXPERIMENTAL SECTION

Fabrication of Porous Layers. Highly ordered TiO_2 nanotube arrays were prepared by anodization of 0.127 mm thick titanium foil (99.99% purity, Sigma Aldrich Chemical Co. Inc.). Ti metal foil was anodized in a two-electrode configuration at a constant applied voltage of 60 V (initial ramping rate 1 V/s, 30 °C) for 1 h in an ethylene glycol solution containing 0.3 wt % NH_4F. To obtain a stable microstructure and the anatase phase, the amorphous TiO_2 nanotube arrays were annealed at 500 °C for 1 h in air. Anatase phase was confirmed by X-ray diffraction (XRD) analysis.[35,36]

Porous Si layers possessing a thickness and porosity similar to the TiO_2 nanotube arrays were prepared by electrochemical etch of a p-type Si wafer (boron doped, resistivity 2.9 Ω · cm, (100) face) in a 1:1 solution (by vol) of 48% aqueous hydrofluoric acid and ethanol. Silicon was etched using a constant current density of 200 mA/cm^2 for 4 min (for the sample of Figure 2), or 100 mA/cm^2 for 4 min (Figure 3 sample). The samples were then annealed in air at 800 °C in a tube furnace for 1 h to form oxidized porous SiO_2.

Optical Interference Spectroscopy. White light from a tungsten lamp (Ocean Optics) was fed through one end of a bifurcated fiber-optic cable and focused through a lens onto the surface of the TiO_2 nanotube array or porous SiO_2 film at normal incidence. The light source was focused onto the center of the sample surface with a spot size approximately 1.5 mm in diameter. Light reflected from the film was collected through the same optics, and the distal end of the bifurcated fiber optic cable was input to a CCD spectrometer (Ocean Optics S-2000). Reflectivity spectra were recorded in the wavelength range 600−1000 nm, with a spectral acquisition time of 100 ms. Typically 50 spectral scans (5 s total integration time) were averaged. The data spacing of the spectrometer was 0.4 nm. To perform the Fourier transform of the spectrum, the *x*-axis was inverted, and a linear interpolation was applied such that the data were spaced evenly in units of nm^{-1}. A Hanning window was applied to the spectrum; it was redimensioned to 4096 data points and zero-padded to the power of two. A discrete Fourier transform using a multidimensional fast prime factor decomposition algorithm from the Wave-

metrics Inc. (www.wavemetrics.com) IGOR program library (FFT) was applied. The Fourier transform of the spectrum yields a peak whose position on the *x*-axis corresponds to the value 2*nL*, corresponding to the effective optical thickness for a reflection mode experiment. The *x*-axis in the FFT spectra displayed in this work is divided by 2, to present the data as a function of *nL*. This peak was monitored in real-time for optical thickness changes during the liquid infiltration and the biosensing experiments.

Porous Materials Characterization. Optical thickness and porosity were measured using optical reflectance spectroscopy in which the value of *nL* (optical thickness) was monitored upon the addition of ethanol. The change in the reflectance spectra as the medium in the pores is changed from air to ethanol is attributed to changes in optical thickness assuming all voids in the film are filled with the liquid. The optical thickness data were least-squares fit to a two component Bruggeman effective medium approximation, yielding values for porosity and thickness of the porous layer.[46] The refractive indices of the host matrix used for the analysis were $n = 2.5$ for TiO_2 and $n = 1.7$ for SiO_2. Refractive index of the liquid ethanol (1.3611 at 22 °C) was measured using a Bausch & Lomb Abbe-3 L refractometer. Thickness and pore size of the porous TiO_2 films were also determined by field emission scanning electron microscopy (FESEM, Phillips XL30).

Stability Test of Porous Materials in Various pH Buffers. Stability of TiO_2 nanotube arrays and porous silica (SiO_2) samples were tested in buffer solutions (VWR, BDH buffers, from pH 2−12) by monitoring the value of optical thickness as a function of time. Phosphate buffered saline (PBS, 1X Cellgro, pH 7.4) was used for a baseline and a rinse between introduction of the other buffer solutions. The refractive indices of the buffer solutions were determined by refractometry (Bausch & Lomb Abbe-3 L) at 22 °C. For time-resolved sensing, a custom-built poly(methyl)methacrylate flow cell was used.[43] The TiO_2 nanotube array or porous SiO_2 substrate was mounted in the flow cell containing inlet and outlet ports and each solution was introduced at a flow rate of 0.7 mL/min using a peristaltic pump (Fisher Scientific). The flow cell contained a transparent window that allowed the acquisition of spectral reflectance data using the spectrometer system described above.

TiO_2 Nanopore Array Biosensing Experiments. The change in optical thickness of the TiO_2 nanotube array was monitored as a function of time, during which a PBS buffer solution of the biomolecule of interest was introduced *via* the flow cell. A baseline was first established with PBS (pH 7.4) for 15−20 min. A solution of 0.1 mg/mL protein A (EMD Calbiochem, 42 kDa) was subsequently introduced and allowed to circulate for 1 h. The cell containing the porous layer was then rinsed with PBS for 15−20 min. The solution of 0.1 mg/mL rabbit IgG (Sigma-Aldrich, >95%, 150 kDa) or 0.1 mg/mL chicken IgG (Sigma-Aldrich, >95%, 150 kDa) was introduced and allowed to circulate in the cell for 1 h. All solutions except the PBS rinsing solution were continuously recirculated from a reservoir with a total volume of ~3 mL during the course of the experiments.

Independent verification of the amount of protein loaded was performed using a bicinchoninic acid (BCA) protein assay (Micro BCA Protein Assay Kit, No. 23235, Pierce division of Thermo Scientific). The TiO_2 nanotube array sample, loaded with protein A as described above, was removed from the flow cell and immersed in a 0.2% solution of Triton X-100 nonionic surfactant (Sigma-Aldrich) in PBS buffer and ultrasonicated for 30 min. The assay was performed following the instructions provided by the manufacturer. To confirm mass balance, separate BCA assays were performed on the protein A loading solutions, both before and after protein loading.

Acknowledgment. This work was supported by the National Science Foundation (Grant No. DMR-0806859), the Korean Regional Technology Innovation Program (Grant No. RTI05-01-02) of the Ministry of Knowledge Economy (MKE), and the Korea Research Foundation (Grant No. KRF-2008-621-D00017).

REFERENCES AND NOTES

1. Lin, V. S.-Y.; Motesharei, K.; Dancil, K. S.; Sailor, M. J.; Ghadiri, M. R. A Porous Silicon-Based Optical Interferometric Biosensor. *Science* **1997**, *278*, 840–843.
2. Dancil, K.-P. S.; Greiner, D. P.; Sailor, M. J. A Porous Silicon Optical Biosensor: Detection of Reversible Binding of IgG to a Protein A-Modified Surface. *J. Am. Chem. Soc.* **1999**, *121*, 7925–7930.
3. Ouyang, H.; Christophersen, M.; Viard, R.; Miller, B. L.; Fauchet, P. M. Macroporous Silicon Microcavities for Macromolecule Detection. *Adv. Funct. Mater.* **2005**, *15*, 1851–1859.
4. Cooper, M. A. Optical Biosensors in Drug Discovery. *Nat. Rev. Drug Discovery* **2002**, *1*, 515–528.
5. González-Martínez, M.; Puchades, R.; Maquieira, A. Optical Immunosensors for Environmental Monitoring: How Far Have We Come. *Anal. Bioanal. Chem.* **2007**, *387*, 205–218.
6. Li, J. L.; Zhao, X. W.; Wei, H. M.; Gu, Z. Z.; Lu, Z. H. Macroporous Ordered Titanium Dioxide (TiO_2) Inverse Opal As a New Label-Free Immunosensor. *Anal. Chim. Acta* **2008**, *625*, 63–69.
7. Brecht, A.; Gauglitz, G. Reflectometric Interference Spectroscopy for Direct Affinity Sensing. *Front. Biosens., II: Pract. Appl.* **1997**, *81*, 1–16.
8. Danelian, E.; Karlen, A.; Karlsson, R.; Winiwarter, S.; Hansson, A.; Lofas, S.; Lennernas, H.; Hamalainen, M. D. SPR Biosensor Studies of the Direct Interaction between 27 Drugs and a Liposome Surface: Correlation with Fraction Absorbed in Humans. *J. Med. Chem.* **2000**, *43*, 2083–2086.
9. Zhang, D.; Crean, G. M.; Flaherty, T.; Shallow, A. Development of Interdigitated Acoustic-Wave Transducers for Biosensor Applications. *Analyst* **1993**, *118*, 429–432.
10. Bataillard, P.; Steffgen, E.; Haemmerli, S.; Manz, A.; Widmer, H. M. An Integrated Silicon Thermopile as Biosensor for the Thermal Monitoring of Glucose, Urea, and Penicillin. *Biosens. Bioelectron.* **1993**, *8*, 89–98.
11. Cooper, M. A. Optical Biosensors: Where Next and How Soon. *Drug Discovery Today* **2006**, *11*, 1061–1067.
12. Gauglitz, G. Direct Optical Sensors: Principles and Selected Applications. *Anal. Bioanal. Chem.* **2005**, *381*, 141–155.
13. Brecht, A.; Gauglitz, G.; Polster, J. Interferometric Immunoassay in a FIA System—A Sensitive and Rapid Approach in Label-free Immunosensing. *Biosens. Bioelectron.* **1993**, *8*, 387–392.
14. Lu, J. H.; Strohsahl, C. M.; Miller, B. L.; Rothberg, L. J. Reflective Interferometric Detection of Label-Free Oligonucleotides. *Anal. Chem.* **2004**, *76*, 4416–4420.
15. Chan, S.; Fauchet, P. M.; Li, Y.; Rothberg, L. J.; Miller, B. L. Porous Silicon Microcavities for Biosensing Applications. *Phys. Status Solidi A: Appl. Res.* **2000**, *182*, 541–546.
16. Li, Y. A.; Wark, A. W.; Lee, H. J.; Corn, R. M. Single-Nucleotide Polymorphism Genotyping by Nanoparticle-Enhanced Surface Plasmon Resonance Imaging Measurements of Surface Ligation Reactions. *Anal. Chem.* **2006**, *78*, 3158–3164.
17. Lee, H. J.; Wark, A. W.; Corn, R. M. Creating Advanced Multifunctional Biosensors with Surface Enzymatic Transformations. *Langmuir* **2006**, *22*, 5241–5250.
18. Homola, J. Present and Future of Surface Plasmon Resonance Biosensors. *Anal. Bioanal. Chem.* **2003**, *377*, 528–539.
19. Janshoff, A.; Dancil, K.-P. S.; Steinem, C.; Greiner, D. P.; Lin, V. S.-Y.; Gurtner, C.; Motesharei, K.; Sailor, M. J.; Ghadiri, M. R. Macroporous p-type Silicon Fabry−Perot layers. Fabrication, Characterization, and Applications in Biosensing. *J. Am. Chem. Soc.* **1998**, *120*, 12108–12116.
20. Stewart, M. P.; Buriak, J. M. Chemical and Biological Applications of Porous Silicon Technology. *Adv. Mater.* **2000**, *12*, 859–869.
21. Hee-Kyung, M.; Ho-Sik, Y.; Cho, S. M. Extremely Sensitive Optical Sensing of Ethanol Using Porous Silicon. *Sens. Actuators, B* **2000**, *B67*, 199–202.
22. Jane, A.; Dronov, R.; Hodges, A.; Voelcker, N. H. Porous Silicon Biosensors on the Advance. *Trends Biotechnol* **2009**, *27*, 230–239.

23. Lees, I. N.; Lin, H.; Canaria, C. A.; Gurtner, C.; Sailor, M. J.; Miskelly, G. M. Chemical Stability of Porous Silicon Surfaces Electrochemically Modified with Functional Alkyl Species. *Langmuir* **2003**, *19*, 9812–9817.
24. Alvarez, S. D.; Derfus, A. M.; Schwartz, M. P.; Bhatia, S. N.; Sailor, M. J. The Compatibility of Hepatocytes with Chemically Modified Porous Silicon with Reference to *in Vitro* Biosensors. *Biomaterials* **2009**, *30*, 26–34.
25. Alvarez, S. D.; Li, C.-P.; Chiang, C. E.; Schuller, I. K.; Sailor, M. J. A Label-Free Porous Alumina Interferometric Immunosensor. *ACS Nano* **2009**, *3*, 3301–3307.
26. Song, Y.-Y.; Schmuki, P. Modulated TiO_2 Nanotube Stacks and Their Use in Interference Sensors. *Electrochem. Commun.* **2010**, *12*, 579–582.
27. Beranek, R.; Hildebrand, H.; Schmuki, P. Self-Organized Porous Titanium Oxide Prepared in H_2SO_4/HF Electrolytes. *Electrochem. Solid State Lett.* **2003**, *6*, B12–B14.
28. Choi, S. Y.; Mamak, M.; von Freymann, G.; Chopra, N.; Ozin, G. A. Mesoporous Bragg Stack Color Tunable Sensors. *Nano Lett.* **2006**, *6*, 2456–2461.
29. Lange, K.; Herold, M.; Scheideler, L.; Geis-Gerstorfer, J.; Wendel, H. P.; Gauglitz, G. Investigation of Initial Pellicle Formation on Modified Titanium Dioxide (TiO_2) Surfaces by Reflectometric Interference Spectroscopy (RIfS) in a Model System. *Dent. Mater.* **2004**, *20*, 814–822.
30. Stein, A. Sphere Templating Methods for Periodic Porous Solids. *Microporous Mesoporous Mater.* **2001**, *44*, 227–239.
31. Huber, K. Pore Volume of Electrolytically Produced Protective Coatings on Aluminum. *J. Coll. Sci.* **1948**, *3*, 197–206.
32. Mont, F. W.; Kim, J. K.; Schubert, M. F.; Schubert, E. F.; Siegel, R. W. High-Refractive-Index TiO_2-Nanoparticle-Loaded Encapsulants for Light-Emitting Diodes. *J. Appl. Phys.* **2008**, *103*, 083120.
33. Macak, J. M.; Tsuchiya, H.; Schmuki, P. High-Aspect-Ratio TiO_2 Nanotubes by Anodization of Titanium. *Angew. Chem., Int. Ed.* **2005**, *44*, 2100–2102.
34. Taveira, L. V.; Macak, J. M.; Tsuchiya, H.; Dick, L. F. P.; Schmuki, P. Initiation and Growth of Self-Organized TiO_2 Nanotubes Anodically Formed in $NH_4F/(NH_4)(_2)SO_4$ Electrolytes. *J. Electrochem. Soc.* **2005**, *152*, B405–B410.
35. Yang, D. J.; Kim, H. G.; Cho, S. J.; Choi, W. Y. Vertically oriented Titania Nanotubes Prepared by Anodic Oxidation on Si Substrates. *IEEE Trans. Nanotechnol.* **2008**, *7*, 131–134.
36. Yang, D. J.; Kim, H. G.; Cho, S. J.; Choi, W. Y. Thickness-Conversion Ratio from Titanium to TiO_2 Nanotube Fabricated by Anodization Method. *Mater. Lett.* **2008**, *62*, 775–779.
37. Macak, J. M.; Sirotna, K.; Schmuki, P. Self-Organized Porous Titanium Oxide Prepared in Na_2SO_4/NaF Electrolytes. *Electrochim. Acta* **2005**, *50*, 3679–3684.
38. Mor, G. K.; Varghese, O. K.; Paulose, M.; Grimes, C. A. Transparent Highly Ordered TiO_2 Nanotube Arrays *via* Anodization of Titanium Thin Films. *Adv. Funct. Mater.* **2005**, *15*, 1291–1296.
39. Mor, G. K.; Shankar, K.; Paulose, M.; Varghese, O. K.; Grimes, C. A. Use of Highly-Ordered TiO_2 Nanotube Arrays in Dye-Sensitized Solar Cells. *Nano Lett.* **2006**, *6*, 215–218.
40. Song, Y. Y.; Hildebrand, H.; Schmuki, P. Photoinduced Release of Active Proteins from TiO_2 Surfaces. *Electrochem. Commun.* **2009**, *11*, 1429–1433.
41. Ghicov, A.; Schmuki, P. Self-Ordering Electrochemistry: A Review on Growth and Functionality of TiO_2 Nanotubes and Other Self-Aligned MO_x Structures. *Chem. Commun.* **2009**, *20*, 2791–2808.
42. Bavykin, D. V.; Milsom, E. V.; Marken, F.; Kim, D. H.; Marsh, D. H.; Riley, D. J.; Walsh, F. C.; El-Abiary, K. H.; Lapkin, A. A. A Novel Cation-Binding TiO_2 Nanotube Substrate for Electrocatalysis and Bioelectrocatalysis. *Electrochem. Commun.* **2005**, *7*, 1050–1058.
43. Schwartz, M. P.; Alvarez, S. D.; Sailor, M. J. A Porous SiO_2 Interferometric Biosensor for Quantitative Determination of Protein Interactions: Binding of Protein A to Immunoglobulins Derived from Different Species. *Anal. Chem.* **2007**, *79*, 327–334.
44. Pacholski, C.; Yu, C.; Miskelly, G. M.; Godin, D.; Sailor, M. J. Reflective Interferometric Fourier Transform Spectroscopy: A Self-Compensating Label-Free Immunosensor Using Double-Layers of Porous SiO_2. *J. Am. Chem. Soc.* **2006**, *128*, 4250–4252.
45. Pacholski, C.; Sartor, M.; Sailor, M. J.; Cunin, F.; Miskelly, G. M. Biosensing Using Porous Silicon Double-Layer Interferometers: Reflective Interferometric Fourier Transform Spectroscopy. *J. Am. Chem. Soc.* **2005**, *127* (33), 11636–11645.
46. Segal, E.; Perelman, L. A.; Cunin, F.; Renzo, F. D.; Devoisselle, J.-M.; Li, Y. Y.; Sailor, M. J. Confinement of Thermoresponsive Hydrogels in Nanostructured Porous Silicon Dioxide Templates. *Adv. Funct. Mater.* **2007**, *17*, 1153–1162.
47. Harlow, E.; Lane, D., *Antibodies: A Laboratory Manual;* Cold Spring Harbor Laboratory: Cold Spring Harbor, N.Y., 1988; p 726.
48. Shin, H. S.; Jang, Y. S.; Lee, Y.; Jung, Y.; Kim, S. B.; Choi, H. C. Photoinduced Self-Assembly of TiO_2 and SiO_2 Nanoparticles on Sidewalls of Single-Walled Carbon Nanotubes. *Adv. Mater.* **2007**, *19*, 2873.
49. Lee, J. A.; Krogman, K. C.; Ma, M.; Hill, R. M.; Hammond, P. T.; Rutledge, G. C. Highly Reactive Multilayer-Assembled TiO_2 Coating on Electrospun Polymer Nanofibers. *Adv. Mater.* **2009**, *21*, 1252–1256.
50. Vörös, J. The Density and Refractive Index of Adsorbing Protein Layers. *Biophys. J.* **2004**, *87*, 553–561.